CCFE
CULHAM CENTRE FOR FUSION ENERGY

UK Atomic Energy Authority

UKAEA-CCFE-PR(21)21

M. Fitzgerald, S. E. Sharapov, P. Siren, E. Tholerus, M. Dreval, G. Szepesi, P. Olivares, T. Jonsson, N. Fil, J. Ferreira, P. Rodrigues, A. Figueiredo, D. Borba, R. Coelho, F. Nabais, J. Mailloux, H.J.C. Oliver, C. Di Troia, F. Napoli, Z. Stancar, R. Dumont, D. Keeling

TAE stability in JET ITB afterglow experiments

TAE stability in JET ITB afterglow experiments

M. Fitzgerald, S. E. Sharapov, P. Siren, E. Tholerus, M. Dreval, G. Szepesi, P. Olivares, T. Jonsson, N. Fil, J. Ferreira, P. Rodrigues, A. Figueiredo, D. Borba, R. Coelho, F. Nabais, J. Mailloux, H.J.C. Oliver, C. Di Troia, F. Napoli, Z. Stancar, R. Dumont, D. Keeling

This is a preprint of a paper submitted for publication in Nuclear Fusion

Toroidal Alfven eigenmode stability in JET internal transport barrier afterglow experiments

M. Fitzgerald[1], S. E. Sharapov[1], P. Siren[2], E. Tholerus[1], M. Dreval[3], G. Szepesi[1], P. Olivares[4], T. Johnson[4], N. Fil[1], J. Ferreira[5], P. Rodrigues[5], A. Figueiredo[5], D. Borba[5], R. Coelho[5], F. Nabais[5], J. Mailloux[1], H.J.C. Oliver[1], C. Di Troia[6], F. Napoli[6], Z. Stancar[1], R. Dumont[7], D. Keeling[1] and JET contributors*

[1]CCFE, Culham Science Centre, Abingdon, OX14 3DB, United Kingdom
[2]Department of Physics, University of Helsinki, 00014 Helsinki, Finland
[3]National Science Centre 'Kharkiv Institute of Physics and Technology', Institute of Plasma Physics, Kharkiv, Ukraine
[4]Fusion Plasma Physics, EES, KTH, SE-10044 Stockholm, Sweden
[5]Instituto de Plasmas e Fusão Nuclear, Instituto Superior Técnico, Universidade de Lisboa, Portugal
[6]ENEA, Fusion and Nuclear Safety Department, C.R. Frascati, Via E. Fermi 45,00044 Frascati (Roma), Italy
[7]CEA, IRFM, F-13108 Saint Paul Lez Durance, France
*See the author list of E. Joffrin et al., Nucl. Fusion 59, 112021 (2019)

Abstract

In this work, we use reduced and perturbative models to examine the stability of toroidal Alfven eigenmodes (TAEs) during the internal transport barrier (ITB) afterglow in JET experiments designed for the observation of alpha driven TAEs. We demonstrate that in JET-like conditions, it is sufficient to use an incompressible cold plasma model for the TAE to reproduce the experimental adiabatic features such as frequency and position. The core-localised modes that are predicted to be most strongly driven by minority ICRH fast ions correspond to the modes observed in the DD experiment, and conversely, modes that are predicted to be not driven are not observed. Linear damping rates due to a variety of mechanisms acting during the afterglow are calculated, and Landau damping by the thermal plasma is shown to be clearly dominant for observed modes. We show that analytical estimates for Landau damping can be too low by an order of magnitude in these experiments, owing to the neglect of higher order sideband resonances. For DT equivalent extrapolations, we conclude that a different set of TAEs that exist towards the edge are more likely to be driven unstable than the DD observed core modes.

Introduction

A great deal of effort and interest has been devoted to demonstrating the possible excitation of Alfvenic instabilities by super-Alfvenic fusion products, particularly alpha particles, a phenomenon that is important to understand and control in future burning plasmas[1]. Recent work on JET [2] has been focused on creating the conditions for unambiguous observation of alpha driven toroidal Alfven eigenmodes (TAEs) by exploiting the long slowing down time of alpha particles and the more rapid thermalisation of beam ions, supporting some existing evidence from JET [3] and TFTR [4]. Afterglow scenarios were designed to achieve a transient maximum performance to generate a large driving fusion alpha population, followed by rapid removal of neutral beam heating to minimize damping effects. Deuterium experiments were conducted to establish high performance ITB scenarios at elevated safety factor with a view that they could be repeated in DT. Although generally omitting ICRH to avoid creating another fast particle population, some of these

experiments deliberately employed ICRH during the afterglow to probe the stability of TAEs, allowing the validation of stability calculations.

In this work, we test the quantitative predictive capability of reduced and perturbative models for TAE stability in a particular JET ITB scenario when supplied by approximate inputs from the available integrated modelling data.

Experimental features reproduced by this workflow include:

- location of rational surfaces
- mode frequency
- mode position
- strongest driven modes
- modes that are absent
- time of onset during afterglow

After demonstrating capabilities in reproducing experimental features in pure deuterium plasma, we present an extrapolation to 50:50 deuterium-tritium plasmas to assess the likelihood of alpha driven TAEs being excited.

Theory

Tokamak plasmas are known to support a broad range of wave phenomena propagating at different characteristic speeds. The local wave dispersion relation includes the Alfven continuum $\omega^2 \approx k_\parallel^2 V_A^2$ and ion-sound continuum $\omega^2 \approx k_\parallel^2 c_S^2$, with V_A and c_s denoting respectively the Alfven and ion-sound speeds. The squared ratio of c_s and V_A depend on β, the ratio of magnetic to thermal pressure. In a conventional tokamak such as JET, these speeds are well-separated and Alfven waves can be identified that are dominated by the interplay between magnetic field tension and plasma inertia, rather than plasma compression. For reactor-relevant conditions, these waves must be kept as small oscillations around an equilibrium with $\frac{\delta B}{B} \ll 1\%$. The toroidally symmetric equilibrium magnetic field balances the pressure of a mostly isotropic plasma as expressed in the fluid picture with the Grad-Shafranov equation

$$R^2 \nabla \cdot \left(\frac{\nabla \psi}{R^2}\right) = -R\mu_0 J_\phi(R,\psi)$$
$$J_\phi(R,\psi) = Rp'(\psi) + ff'(\psi)/\mu_0 R \qquad (1)$$

where the poloidal flux functions correspond to the pressure force $-\nabla p = -p'(\psi)\nabla\psi$ and the covariant toroidal magnetic field $RB_\phi = f(\psi)$. In the kinetic picture on collisionless timescales, a particle distribution function is in equilibrium if and only if it can be written in terms of particle orbit constants of motion

$$F = F(E, \mu, P_\phi; \sigma) \qquad (2)$$

for energy E, magnetic moment $\mu = \frac{\frac{1}{2}mv_\perp^2}{B} + O\left(\frac{\rho}{L}\right)$, toroidal canonical momentum $P_\phi = mRv_\phi + Ze\psi$ and $\sigma \equiv sign\ (v_\parallel)$. The above expressions correspond to sign conventions [5] where poloidal flux $\boldsymbol{B_p} \equiv \nabla\psi \times \nabla\phi$ and toroidal direction $\hat{R} \times \hat{\phi} = \hat{Z}$.

The two pictures, represented by equations (1) and (2), are reconciled for the majority thermal plasma with zero orbit width where $F = F(E, \psi)$. The fast particle distributions associated with NBI, ICRH or the fusion products cannot be said to satisfy this assumption in JET-like conditions; NBI and

ICRH orbits can exhibit strong directionality favouring a given invariant pitch $\Lambda \equiv \frac{\mu B_0}{E}$ and all fast particles exhibit a finite orbit width through P_ϕ. Although these quantities feature naturally in the kinetic theory, integrated modelling focusing on flux-surface average quantities tends to ignore these effects for computational convenience with varying levels of justification in current tokamaks. As an example: for large aspect ratio, a fast pressure approximation [6] is justified to capture the fast particle forces in the Grad-Shafranov equation.

The TAE was first identified [7] as a class of discrete oscillatory solution to the linearized ideal MHD equations in the limit of small β. These global eigenmodes exist within the TAE gap of the Alfven continuum at angular frequencies close to

$$\omega_{TAE} = \frac{V_A}{2qR} \tag{3}$$

These incompressible ideal solutions from the fluid theory may also be found in the kinetic theory when solving for the "adiabatic" terms in the linearized gyrokinetic equation, or by assuming a cold plasma dispersion relation for the given field and density. Real and imaginary corrections to the TAE eigenfrequency and mode structure come from non-ideal effects such as resonant wave-particle interaction, collisions, finite orbit width and finite Larmor radius [8][9]. When these effects are weak, they provide only drive, damping and frequency corrections to what are in essence ideal MHD solutions, inviting a perturbative approach.

Resonant wave-particle interaction is computed perturbatively with linear codes such as CASTOR-K [10] and NOVA-K [11], and nonlinear codes such as HAGIS [12] and HALO [13]. These perturbative calculations require inputs of the ideal eigenmodes from linear MHD codes such as MISHKA [14] and CASTOR [15].

The further non-ideal contributions from finite Larmor radius and parallel electric field lead to the coupling with kinetic Alfven waves with a combined local dispersion relation

$$\omega^2 = k_\parallel^2 V_A^2 \left[1 + k_\perp^2 \rho_i^2 \left(\frac{3}{4} + \frac{T_e}{T_i}\left(1 - i\delta(\nu_e)\right)\right)\right] \tag{4}$$

with ion Larmor radius $\rho_i = (m_i T_i)^{1/2}/eB$ and collisional dissipation $\delta(\nu_e)$, and a corresponding modification to the global TAE wave equation. The collisional dissipation captures the passing electron resistive losses and can be computed from the collision frequency ν_e with trapped electrons.

This modified kinetic TAE wave equation resembles the resistive MHD equations but with a complex number substituting for conventional resistivity, allowing non-perturbative computation of some nonideal effects in CASTOR [9]. The coupling between kinetic Alfven waves and TAEs leads to radiative damping of TAEs when their frequencies lie below the TAE gap frequency equation (3) [16]. Full non-perturbative calculations can also be performed using gyrokinetic or hybrid codes [17][18][19] which attempt to solve for all ideal and non-ideal effects simultaneously, including the difficult to resolve resonant wave-particle interaction. The GTC code [20] is a recent example of a gyrokinetic code applied to TAEs. For slowly growing/decaying modes, power transfer between waves and particles occurs for a small fraction of particles satisfying the resonance condition [21]

$$0 = n\langle\omega_\phi\rangle + p\omega_\theta - \omega \tag{5}$$

where n is the wave toroidal mode number, $\langle\omega_\phi\rangle$ and ω_θ are the bounce-averaged $\langle..\rangle$ toroidal and poloidal frequencies of the particles, and p is an integer that labels each Fourier component in the time varying power transfer. For deeply passing particles and small orbit width, the strongest Fourier component occurs when $p \approx m$ the poloidal mode number for one of the eigenmode harmonics, corresponding to when $\omega \approx \boldsymbol{k}\cdot\boldsymbol{v}$ for that Fourier component. Analytical expressions [22] of alpha drive and ion Landau damping for of TAEs have been derived for this lowest order power transfer corresponding to the conditions $v_\parallel = V_A$ and $v_\parallel = V_A/3$. More generally, the linear growth rate γ_L depends on the distribution function gradients at resonance

$$\gamma_L = \int d^3x d^3v \sum_\sigma \sum_p \frac{\delta\gamma(x,v;p,\sigma)}{n\langle\omega_\phi\rangle + p\omega_\theta - \omega}$$
$$\delta\gamma(x,v;p,\sigma) \propto \omega\left(\frac{\partial F}{\partial E}\right)_{\mu,P_\phi} - n\left(\frac{\partial F}{\partial P_\phi}\right)_{E,\mu} \quad (6)$$

On JET [23], resonant wave-particle interaction with TAEs occurs between ICRH, NBI, fusion products and thermal plasma species. For typical JET magnetic fields and densities, the ion velocities present in the NBI and thermal distributions fall below V_A and do not contribute drive to TAEs. Drive of TAEs observed on JET is almost exclusively provided by ICRH.

In the sections that follow, we compare predictions of this stability theory to experimental data on an existing DD discharge 92416 during the afterglow, and provide extrapolations of TAE stability in DT for the best performing scenario, which was achieved in discharge 96852.

Predictions for the JET ITB afterglow

Overview of the JET ITB afterglow

Recent scenario development of JET ITBs has been described previously [2][24], but here we give a brief summary of key features of the shot 92416. The plasma is a monotonic $q(\psi)$ low shear discharge with $B_{vac} = 3.4T$ and $I_p = 2.5MA$ operating at elevated $q_0 \approx 2$. NBI heating exceeding approximately 25MW for JET with the ITER-like (metal) wall can lead to the formation of an internal transport barrier at the $q = 2$ surface, with some sensitivity on timing and density, the latter being set as low as shine-through limits allow. Strong density and ion temperature peaking are a feature of this scenario which can result in ion/electron temperature ratios of order $T_i \approx 2T_e$when discharges are successful at producing an ITB. Figure 1 gives the measured magnetic probe signal at the expected TAE gap frequency before and after the full NBI power phase. Three modes are observed at 46.2s with toroidal mode numbers n=4,5,6. These modes occur during a period when the NBI has been stopped and the plasma is cooling. ICRH is maintained during the afterglow so as to

deliberately destabilize TAEs. A higher performance version of the same shot has been developed to be repeated in DT, 96852, with no ICRH and peak transient neutron rate $R_{NT} = 2.45 \times 10^{16}$.

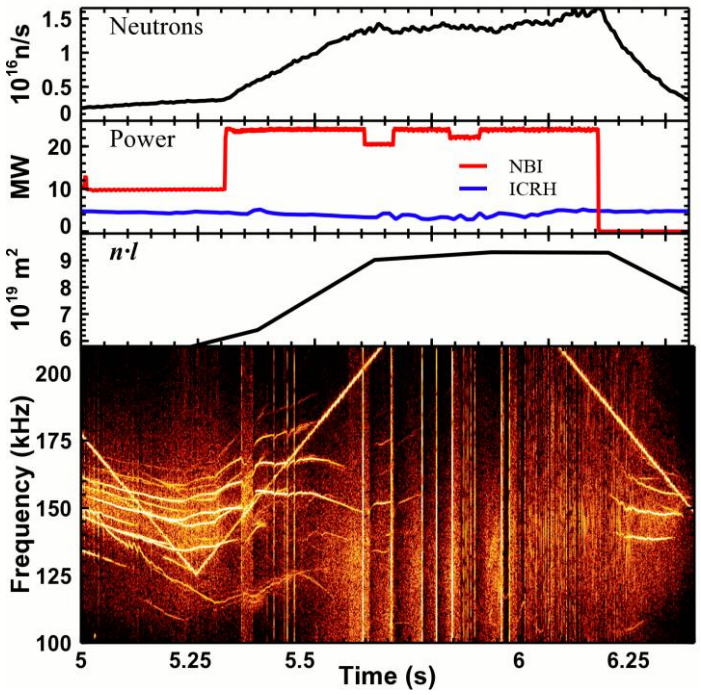

Figure 1: JET shot 92416 afterglow scenario details (above) magnetic spectrum (below). 40s has been subtracted from the time base.

Fluid equilibrium reconstruction

The linear TAE spectrum depends sensitively on the equilibrium, particularly on the q-profile. Inference of equilibrium is provided on JET using the EFIT code [25]. However during the afterglow, MSE measurements are unavailable. A large variation in q-profiles between equally valid EFIT solutions is possible if internal current profile constraints are absent [26]. Considering both free functions in the Grad-Shafranov equation (equation (1)), detailed information on $p'(\psi)$ is available via measurements and fast ion modelling, but very little is available to constrain $ff'(\psi)$ without MSE or computed parallel current constraint. Over-fitting the pressure pedestal in these ITB cases led to implausibly low safety factor in the core. For this study, both free flux functions $p'(\psi)$ and $ff'(\psi)$ were instead parametrised by simple quadratic polynomials, and experimental thermal pressure and computed fast pressure from TRANSP [27] were used as input constraints. Although it is likely that this approach does not capture equilibrium features in the pedestal, our focus was to faithfully capture the core q-profile.

MHD spectroscopy was used to validate this procedure for our ITB cases of interest. The locations of instabilities, likely to be tearing modes, were identified using cross-correlation between electron cyclotron emission and Mirnov coil data. Two modes, with $n = 2$ and $n = 3$, were identified at different times. This provided measurements of the $q = 2$ surface at major radius $R = 3.15 \pm 0.05m$ and $q = \frac{7}{3}$ at $R = 3.45 \pm 0.05m$ at times 45.52s and 45.69s respectively, before the time of interest 46.2s. A comparison with the reconstruction is presented in Figure 2.

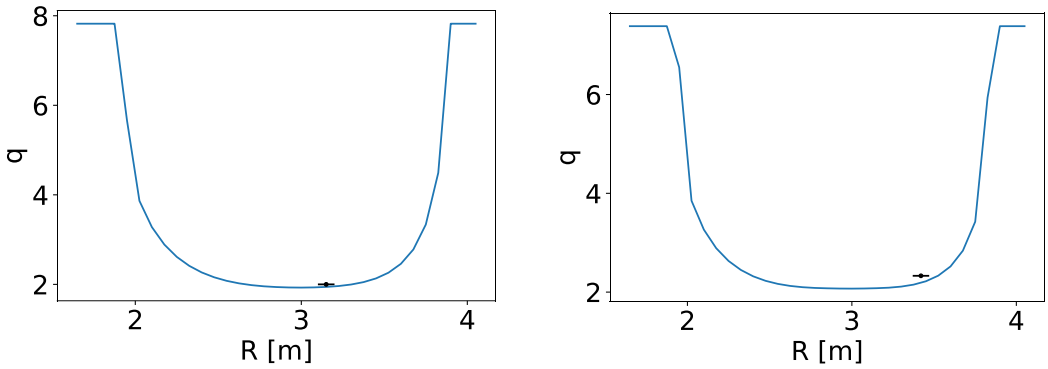

Figure 2: Comparison of q-profile of EFIT reconstruction (curves) to measured midplane position (point with errorbar) of tearing modes at 45.52s (left) and 45.69s (right) in JET shot 92416

The reconstructed position of the $q = 2$ surface also agrees with the position of the ITB; an integer value always appears to be necessary for JET ITBs with monotonic shear [28]. A steady decay from $q_{min} = 2$ to $q_{min} = 1$ can also be inferred from Alfven cascades after the time of interest, beginning from 46.5s.

Incompressible linear stability

Magnetics signals close to the TAE gap frequency computed with equation (3) were observed both before the time of peak performance and during the afterglow (Figure 1). A reconstructed equilibrium at the time of appearance during the afterglow was obtained at 46.2s and metric elements of the straight field line coordinates were obtained with HELENA [29] for input to linear MHD calculations.

As mentioned previously, the three experimentally observed modes had toroidal mode numbers $n = 4,5,6$. On JET, the convention for positive toroidal mode number indicates a mode propagating in the ion-diamagnetic direction for peaked core pressure, which corresponds to a toroidal wave number $n\nabla\xi$ using the $\hat{R} \times \hat{Z} = \hat{\xi}$ sign convention. Plasma current, toroidal field, toroidal rotation and neutral beams are all in the same toroidal direction as the propagating modes.

The straight field line metric elements from HELENA and a normalized mass density profile were used as inputs for the incompressible linear MHD code MISHKA-1. The mass density was approximated on the assumption of 100% deuterium with number density from fitted experimental LIDAR and Thompson scattering electron number density data. A range of TAE eigenmode solutions were found for the for toroidal mode numbers $n = 4,5,6$. The rotation of the plasma at the location of the observed modes was estimated as the difference in frequency for adjacent mode numbers, owing to the expected Doppler shift $\omega_{lab} = \omega_{plasma} + n\Omega$ giving a rotational frequency at the modes of $\Omega/2\pi = 10kHz$, assuming the modes are in similar location with similar rotation.

The range of eigenmodes predicted from the incompressible theory for the measured profiles and assumed rotation in the lab frame occurred in the frequency range 135-165kHz. Solutions in this range of frequencies have been overlayed onto the measured magnetic spectrum in Figure 3. Once toroidal mode number is accounted for, three predicted solutions are found that correspond to within 1-2% of the observed signals. This supports the conclusion that the adiabatic properties of the modes are well modelled by TAEs from the incompressible theory.

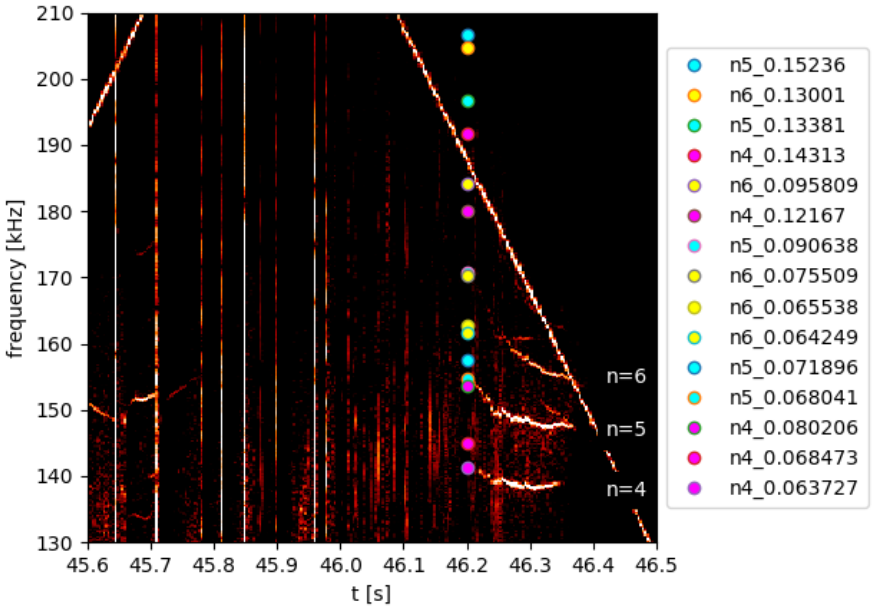

Figure 3: JET shot 92416 magnetic spectrum with MISHKA TAE solutions overlayed. All frequencies are given in the lab frame assuming a toroidal rotation of 10kHz. Modes are coloured by toroidal mode number and labelled with their normalized eigenvalue as "n{mode number}_$\{\omega/\omega_A\}^2$"

The eigenmodes that most resemble experimental observations correspond with archetypical core-localised TAEs which are characteristic of low magnetic shear in the analytical theory [30] and found to be most unstable in ITER baseline calculations [31,32]. These three modes are also of "ballooning" type, where the frequencies are found within the lower half of the TAE gap in the Alfven continuum, and the mode positions are weighted towards the outboard side of the midplane. The MHD prediction of the eigenmode is presented in Figure 4 along with reflectometer measurements. The reflectometer measures density fluctuations at a given probed frequency. The TAEs observed on the magnetics are clearly evident in the density fluctuations, with the n=4 and n=5 modes shown in Figure 4. The probed frequency is scanned in time, altering the radial position where the density fluctuation is measured, depending on the cut-off in the local dispersion relation. The inferred radial position is shown below the spectrum. The n=5 is measured at an outboard major radius of $R \approx 3.33m$ which agrees with MISHKA predictions.

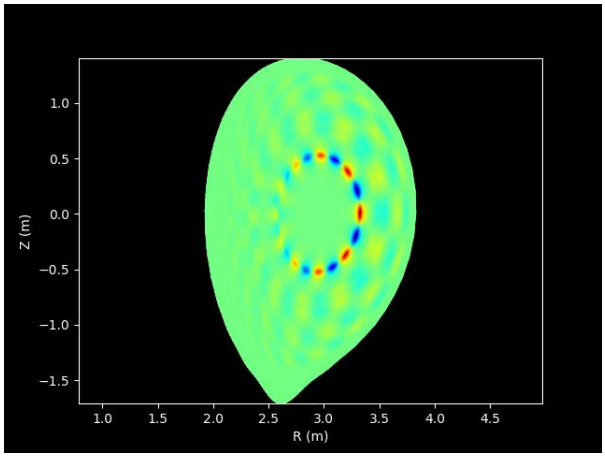

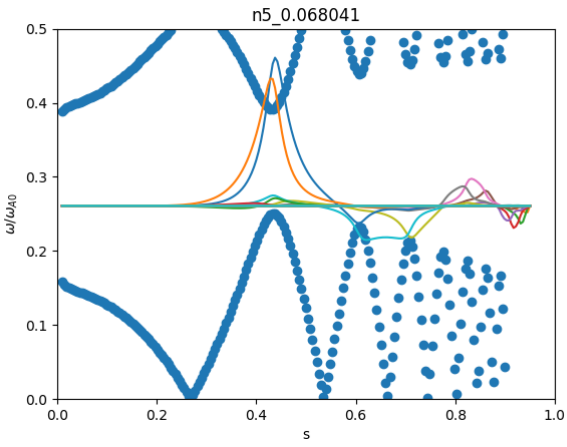

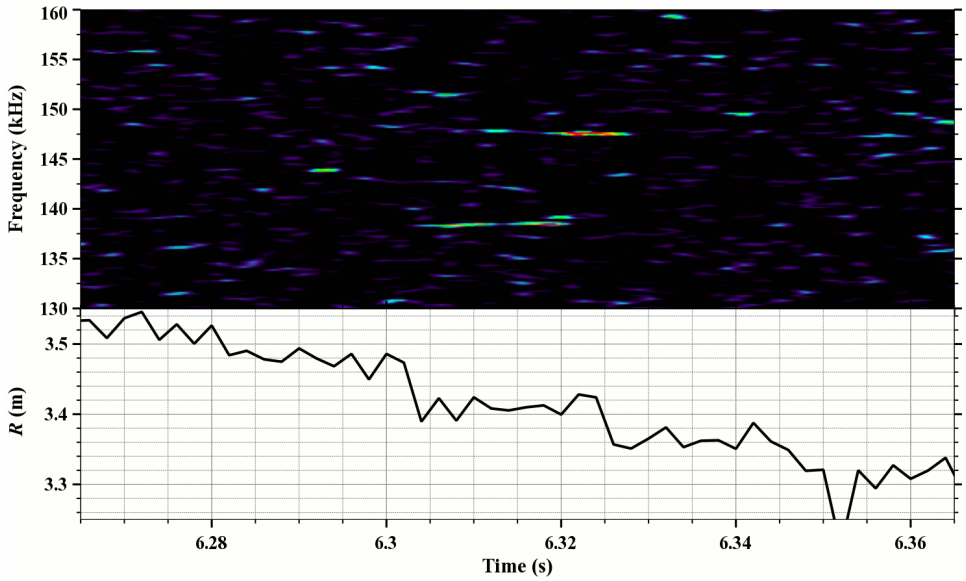

Figure 4: MISHKA 2D perturbed radial velocity sV^1 where $s = \sqrt{\bar{\psi}}$ (top left) and the 1D equivalent superimposed on the Alfven continuum (top right) for n=5 eigenmode observed. Reflectometry measurements (bottom) give the position of the TAEs in JET shot 92416. 40s has been subtracted from the time base.

Kinetic ICRH minority and NBI equilibrium

Radio-frequency heating of a hydrogen minority was included in shot 92416 for the purpose of probing TAE stability during the afterglow. Calculations of resonant wave-particle TAE drive requires the input of the minority hydrogen distribution of the form expressed in equation (2) to capture effects of finite orbit width and strong anisotropy. The SELFO code [33] was used to solve the quasilinear equations for the ICRH fast proton distribution in constants of motion. Additionally, NBI heating was present during the high-performance phase, and then turned off to decrease resonant wave-particle TAE damping. The ASCOT code [34] was used to solve the Fokker-Plank equation for the fast deuterons in position and velocity coordinates, and then converted to the equilibrium form given by equation (2), capturing all finite Larmor orbit width and anisotropy features present in the beam distributions.

The output of distribution function modelling is presented in Figure 5 and Figure 6. Both distributions show significant anisotropy, particularly the SELFO distribution which is strongly peaked around $\Lambda = \frac{\mu B_0}{E} = 1$ as expected from the quasi-linear theory applied to on-axis minority heating.

Being Monte-Carlo solutions, the distributions feature significant Monte-Carlo noise, particularly along edges of the topological orbit boundaries that are sparsely populated in reality and poorly resolved in computation. Although perfectly valid as collisionless equilibrium distribution functions by virtue of their representation $F = F(E, \mu, P_\phi; \sigma)$, they are not physically realisable because they violate a smoothness condition in the Fokker-Plank equation; drag and diffusion terms in the collision operators would become large around any sharp features in the equilibrium, immediately smoothing the distribution. Stability calculations using such unphysical equilibria will produce numerically converged but physically irrelevant results if these gradients happen to occur near the resonance condition. Under these circumstances, numerical convergence of the entire integrated stability calculation would require convergence of the derivatives of the 3D distribution function in the Monte-Carlo simulations.

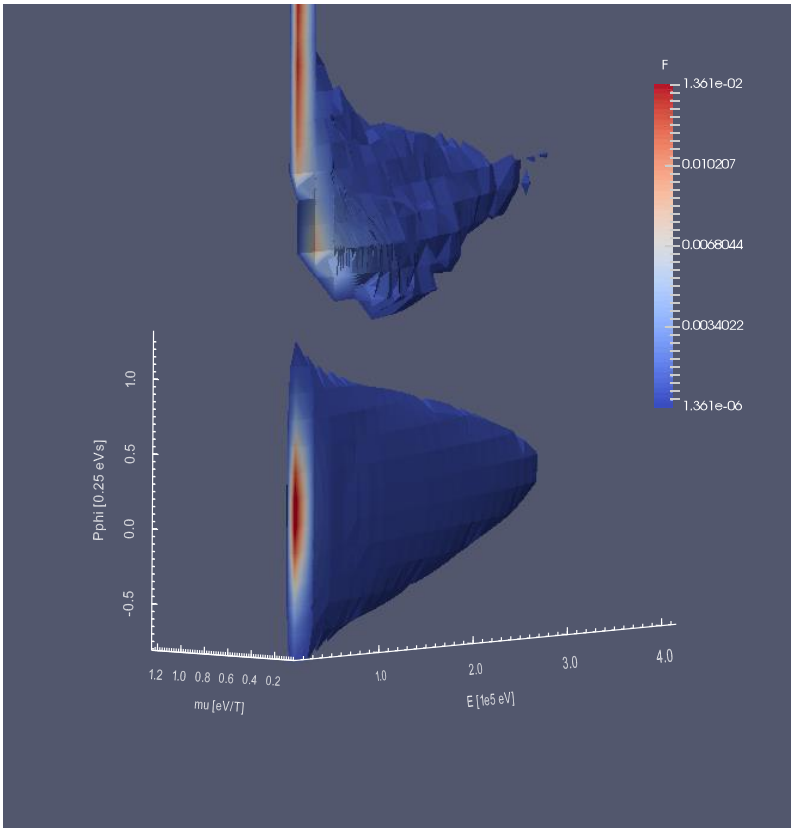

Figure 5: SELFO ICRH distribution function at 46.1s (above) and analytical fitted form (below)

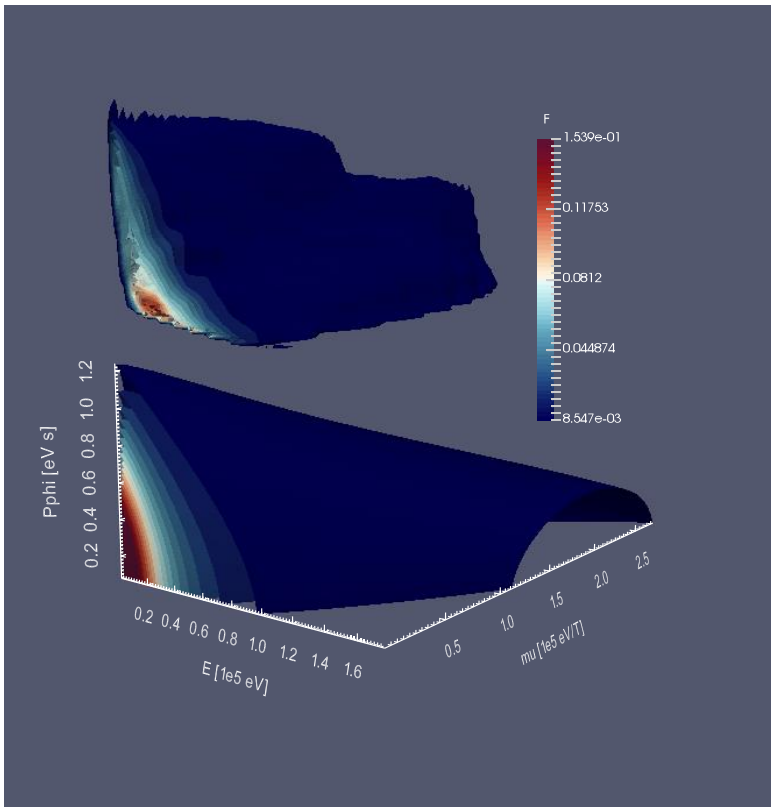

Figure 6: ASCOT NBI distribution function at 46.1s (above) and analytical fitted form (below)

In order to de-couple numerical convergence of heating codes from stability calculations whilst retaining finite orbit width and anisotropic effects, physically motivated parametric distribution functions derived in [35][36] were adopted

$$F_{ICRH}\left(E[eV],\mu[eV/T],P_\phi[eVs]\right) \equiv N\frac{\left(1.0+\frac{\mu/E}{\lambda_0}\right)\left(\frac{E}{T}\right)^{\alpha}}{\sqrt{2\pi}}E^{-\frac{3}{2}}e^{-\frac{\left(P_\phi-P_0\right)^2}{\Delta P^2}}e^{-\frac{E}{T}\left(1+\frac{\left(\frac{\mu}{E}-\lambda_0\right)^2}{\Delta\lambda^2}\right)} \quad (7)$$

$$F_{NBI}\left(E[eV],\mu[eV/T],P_\phi[eVs]\right) \equiv N\frac{1}{\sqrt{2\pi}}\frac{1}{E^{\frac{3}{2}}+E_C^{\frac{3}{2}}}e^{-\frac{\left(P_\phi-P_0\right)^2}{\Delta P^2}}e^{-\frac{E}{T}\left(\frac{\left(\frac{\mu}{E}-\lambda_0\right)^2}{\Delta\lambda^2}\right)} \quad (8)$$

The free parameters $T,\lambda_0,\Delta\lambda,P_0,\Delta P,N,E_c,\alpha$ were manually fitted to best reproduce the functions $\left(\frac{\partial F}{\partial E}\right)_{\mu,P_\phi}$ and $\left(\frac{\partial F}{\partial P_\phi}\right)_{E,\mu}$ and the integral velocity moments of the distribution, the density and pressure. The parameters used are listed in Table 1, with the resulting distributions plotted in Figure 5 and Figure 6. Even after this tedious procedure, the fitted ICRH distribution had missing outboard features in the density profile, and a resulting fitted pressure that was 30% too high compared with SELFO outputs. No automatic tools were available to perform fits to ICRH/NBI Monte-Carlo output, systematically quantifying the fitting error and propagating implications. Moreover, as the analytical forms do not capture all processes modelled in Monte-Carlo heating codes, trade-off decisions are involved in which features of the distribution function are most important to capture. We deem this aspect of the integrated fast-ion stability modelling an important unsolved problem beyond the scope of this study.

Table 1: Fitted parameters for analytical representation of heating code output, giving the distribution functions in S.I. units.

	$\top(eV)$	$\lambda_0(T^{-1})$	$\Delta\lambda(T^{-1})$	$P_0\ (eVs)$	$\Delta P(eVs)$	$E_c(eV)$	α	N
ICRH	30000	0.3	0.05	0.04375	0.143125	-	0.8	0.3×10^6
NBI $\sigma=+$	29197.1	0.18	0.3	0.0	0.5525	25000	0.0	2.5×10^6
NBI $\sigma=-$	28090.5	0.18	0.3	0.0	0.6744	25000	0.0	2.5×10^6

Resonant ICRH linear stability

Full-orbit calculations of linear wave-particle interaction were made with HALO using the fitted ICRH distribution approximation, along with the equilibrium and incompressible eigenmodes from the presented EFIT/HELENA/MISHKA analysis. The resulting linear growth rates are presented in Figure 7. Even before the consideration of damping mechanisms, some important experimental features are evident. Firstly, the three strongest linearly driven MISHKA eigenmodes correspond exactly to those observed during the afterglow in Figure 3, with the most unstable of the three modes, the n=5, appearing first, and the remaining two also appearing in order. Secondly, although most of the ICRH fast ion energy is localised in the core, the calculations correctly predict a very significant difference between inboard and outboard TAE stability for the core modes. This is due to the anisotropy of the fitted ICRH distribution function consisting of mainly trapped particles with banana tips along $R=R_{mag}$, with orbits that remain on the low field side. Experimentally, the inboard TAEs are not evident in Figure 3, with no modes observed above 170kHz. This is despite inboard TAEs not being affected by radiative damping.

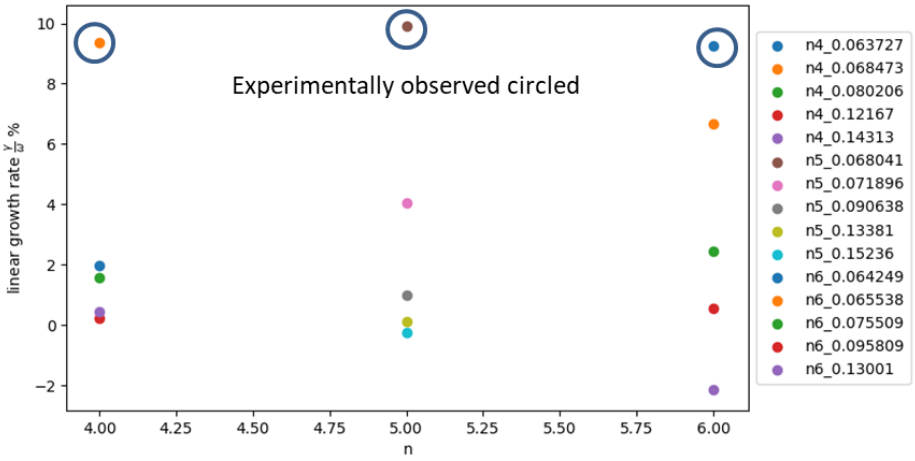

Figure 7: HALO wave-particle interaction calculations for the drive of incompressible TAEs by hydrogen minority ions

Linear drive and damping during the DD afterglow

A detailed examination of the core ballooning n=5 TAE observed during the DD afterglow was conducted to understand the strongest contributions to linear drive and damping. Smooth experimental fits of 1D electron and ion temperature were used for the calculation of bulk thermal plasma effects. The HALO code was used for full-orbit perturbative calculations of ICRH drive, NBI damping and thermal ion Landau damping. CASTOR-K was used for drift-kinetic calculations of ion Landau damping. For non-perturbative calculations of damping, CASTOR was used to compute the radiative damping using the complex resistivity approximation, whilst both radiative damping and all other thermal plasma effects were computed with GTC.

For the CASTOR complex resistivity calculation, values were taken at the position of the eigenmode: R_0=2.96m, R=3.30m, Ti=5.18keV,Te=3.40keV,q=1.86,|B|=3.06T, $|B_0|$=3.4T , $n_e = 3.52 \times 10^{19} m^{-3}$,$n_{e0} = 4.93 \times 10^{19} m^{-3}$. The resistivity normalized to Alfven frequency on axis ω_A for CASTOR input [32] is given by

$$\omega_{TAE} = \frac{V_A(R)}{2qR}, \omega_A = \frac{V_A(R_0)}{R_0}$$
$$\xi = \frac{3}{4} + \frac{T_e}{T_i}(1 - i\delta)$$
$$\eta = i\xi \left(\frac{\omega}{\omega_A}\right)\left(\frac{\omega}{\omega_{TAE}}\right)^2 \left(\frac{\rho_i}{R_0}\right)^2 \quad (9)$$

giving $Im\{\eta\} = 4.9 \times 10^{-7}$. The inclusion of this imaginary component in the resistivity results in a combination of kinetic Alfven wave and TAE in the CASTOR solution. Because the kinetic Alfven wave is very sensitive to the wave dissipation δ, increasing the dissipation suppresses the kinetic Alfven wave, leaving only a damped TAE. Extrapolation of TAE damping to $\delta = 0$ gives the inherent radiative damping of the TAE. The result of such a scanning process, shown in Figure 8, leads to a radiative damping value of $\frac{\gamma}{\omega} = -1\%$.

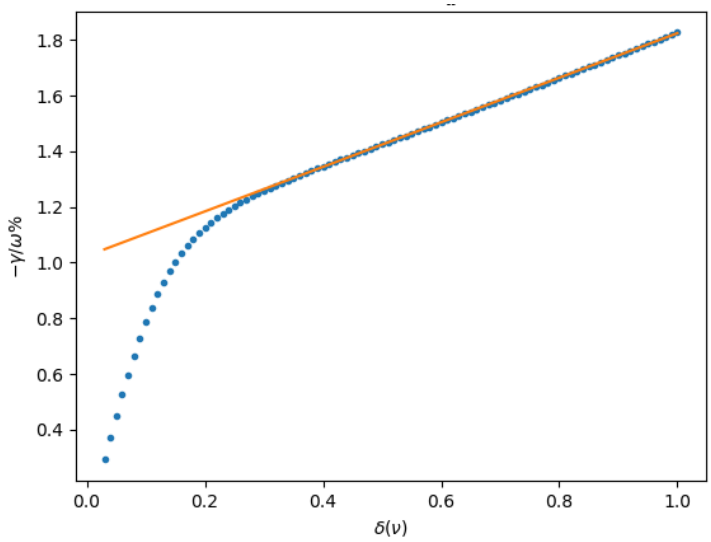

Figure 8: CASTOR scan of wave dissipation to obtain the radiative damping of the n=5 TAE mode of interest

To obtain a second non-perturbative calculation of thermal damping, the linear gyrokinetic response of thermal plasma was scanned using a model antenna within the GTC code. A resonance was identified with similar spatial structure to the MISHKA result and 7% difference in real frequency. The quality factor was determined by fitting the antenna response to an idealised cavity resonator transfer function

$$|H(\omega)|^2 \propto \frac{1}{(\omega - \omega_0)^2 + \gamma^2} \tag{10}$$

with the resulting fit shown in Figure 9. This gave a value of $\frac{\gamma}{\omega} = -5.43 \pm 0.75\%$, which includes all thermal plasma contributions, including radiative damping and ion Landau damping.

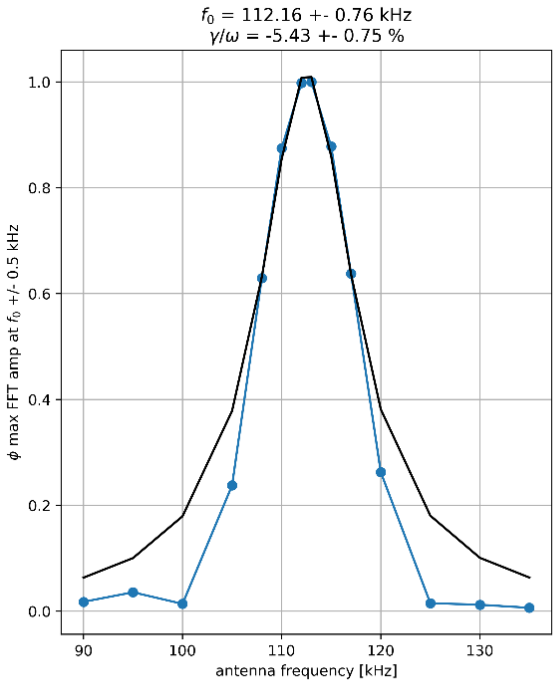

Figure 9: GTC results of non-perturbative thermal plasma response to an antenna for the n=5 mode of interest. The blue points are GTC and the black is a fitted cavity resonator transfer function

Analytical approximations for ion Landau damping were also computed. Analytical theory of resonant wave-particle interaction with TAEs [22] assuming zero orbit width gives the following expression for damping due to a Maxwellian population

$$\frac{\gamma}{\omega} = -q^2\beta\left[g(\lambda) + g\left(\frac{\lambda}{3}\right)\right]$$

$$g(\lambda) = \frac{\pi^{\frac{1}{2}}}{2}\lambda(1 + 2\lambda^2 + 2\lambda^4)e^{-\lambda^2}$$

$$\lambda \equiv \frac{V_T}{V_A}\,, \qquad V_T \equiv \sqrt{\frac{2T_i}{m}}\,,\ \beta = 2\mu_0 n_i T_i/B^2 \tag{11}$$

The analytical expression in equation (11) captures the lowest order TAE resonances $v_\parallel = V_A$ and $v_\parallel = V_A/3$ in the terms $g(\lambda)$ and $g\left(\frac{\lambda}{3}\right)$ respectively.

A summary of linear findings during the afterglow are presented in Figure 10. It is immediately clear that the bulk thermal plasma, through the nonideal resonant effect of ion Landau damping, is providing the majority of TAE suppression for this core mode. NBI damping is found to be a comparatively small contribution to the total damping with $\frac{\gamma}{\omega} \sim -0.2\%$. There is good agreement between the perturbative models CASTOR-K and HALO and the non-perturbative model GTC that the bulk thermal plasma is responsible for suppressing the core TAEs during the high-performance phase.

Given that TAEs are suppressed at 46.1s and only appear at 46.2s, the ICRH drive calculations are clearly too high by a factor 1.2-1.3 unless further damping mechanisms have been overlooked. Antenna measurements at later times in the pulse [24] seem to be fully explained by radiative damping and don't suggest any further damping mechanisms not already mentioned. We conjecture that this is mostly to do with deficiencies in details of the fitted SELFO distribution function, as our analytical fits to the Monte-Carlo distribution could not simultaneously match fast density, fast pressure, and local gradients.

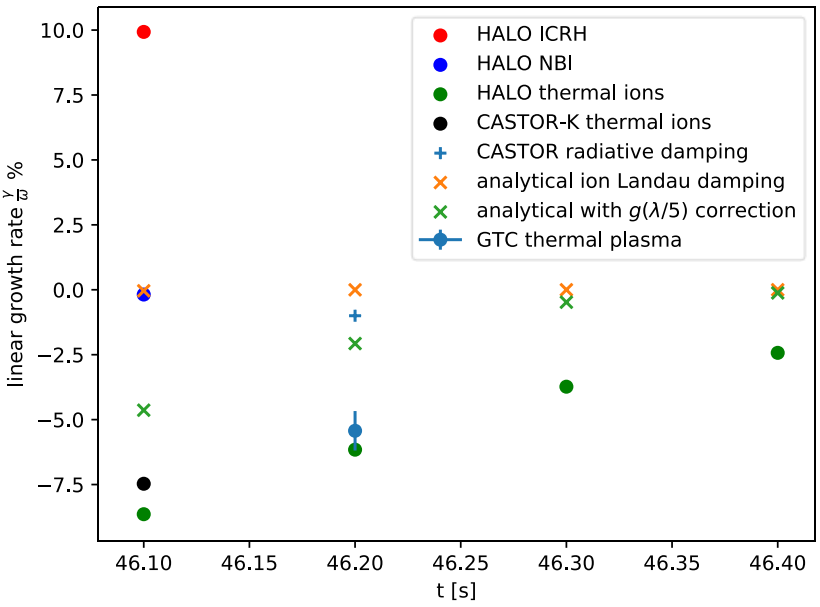

Figure 10: summary of linear findings during the afterglow. TAE appears at 46.2s

Breakdown of analytical theory in JET limit

The difference is striking between the analytical estimate of ion Landau damping and the linear computation in three different models – drift-kinetic, gyrokinetic and full orbit. The idealised expression given by equation (11) includes only deeply passing particle resonances, and only includes the lowest order bounce harmonics $v_{\parallel} = V_A$ and $v_{\parallel} = V_A/3$. Both these approximations are very significant under these conditions. To illustrate this point, the HALO code was run with fixed wave amplitude and unperturbed orbits to accumulate the power transfer for each δf marker in the phase space hypercube E, μ, P_ϕ and the results are presented in Figure 11. Although the whole hyper-cube is populated in the simulation, only a selection of markers with appreciable power transfer is shown to assist with visualising the key features. Most of the blue markers are where non-resonant random power transfer occurs. Poloidal flux in our convention is positive and small at the magnetic axis, and positive and large at the plasma edge, indicating that low values of $P_\phi = Ze\psi + O\left(\frac{\rho}{L}\right)$ are near the bottom of Figure 11. Furthermore, co-passing particles travel in the negative ϕ direction on JET, meaning that fast co-passing particles are found at the very bottom of the figure.

For particles at low $\Lambda \equiv \mu B_0/E$, the particles are passing, and a thin surface corresponding to $P_\phi = mRv_\phi + Ze\psi_{TAE}$ is traced, owing to the TAE peaking at one value of poloidal flux ψ_{TAE} , and this radial position must be encountered by the particle over its orbit to perform appreciable work on the mode. Conversely, for slow strongly trapped particles at high Λ, higher poloidal harmonics of the TAE become an alternative way that stagnant particles may persistently transfer power to the TAE even away from its main radial peak. These two effects give the overall shape of the non-zero power transfer surface. On each of these poloidal harmonic surfaces, the subset of particles with the strongest power transfer are in resonance and form clear lines. A succession of energies associated with a resonance condition are 585keV, 65keV, 23keV and 12keV corresponding to $V_A, \frac{V_A}{3}, \frac{V_A}{5}, \frac{V_A}{7}$ respectively. Unsurprisingly, the V_A plays no role for a thermal plasma at tens of keV, however more surprising is that $\frac{V_A}{3}$ has a weak contribution. The $\frac{V_A}{5}, \frac{V_A}{7}$ lines are the main passing particle

resonances, with $\frac{V_A}{5}$ the most important. Therefore, a large missing term resembling $g\left(\frac{\lambda}{5}\right)$ in equation (11) appears to be appropriate for JET like conditions, and explains much of the discrepancy with the analytical theory of ion Landau damping. This suggests a gross under-estimate of ion Landau damping in some previous analytical JET work [37]. Connor et al. [9] anticipated that because of ellipticity and Shafranov shift, the work done by passing particles $v_D \cdot \delta E$, when integrated over an orbit, contains small amounts of poloidal harmonics such as $k_\parallel = 5/2qR$ and $k_\parallel = 7/2qR$ corresponding to $\frac{V_A}{5}$, $\frac{V_A}{7}$. They concluded that a better approximation to ion Landau damping is given by

$$\frac{\gamma}{\omega} = -q^2\beta\left[g\left(\frac{\lambda}{3}\right) + \left[\frac{3}{4}\Delta' + \frac{3}{4}\frac{E}{r} - \frac{5}{4}E'\right]^2 g\left(\frac{\lambda}{5}\right) + \left[\frac{7}{12}E' - \frac{3}{4}\frac{E}{r}\right]^2 g\left(\frac{\lambda}{7}\right)\right] \qquad (13)$$

with $\Delta(r)$ the equilibrium Shafranov shift, $E/r = (\kappa - 1)/(\kappa + 1)$ the ellipticity parameter, and dash denotes radial gradient. However, we have not verified that ellipticity and Shafranov shift are the main causes for the sideband resonance in this case and no clear account is made for trapped particles. The accuracy of this more detailed expression should be investigated in more detail in future work.

As has been noted previously [38], both co and counter passing particles resonate with the TAE owing to the pair of poloidal harmonics travelling opposite poloidal directions, so the $\frac{V_A}{5}$ resonance can be observed on both co and counter passing branches of $P_\phi \approx Ze\psi_{TAE}$ in Figure 11.

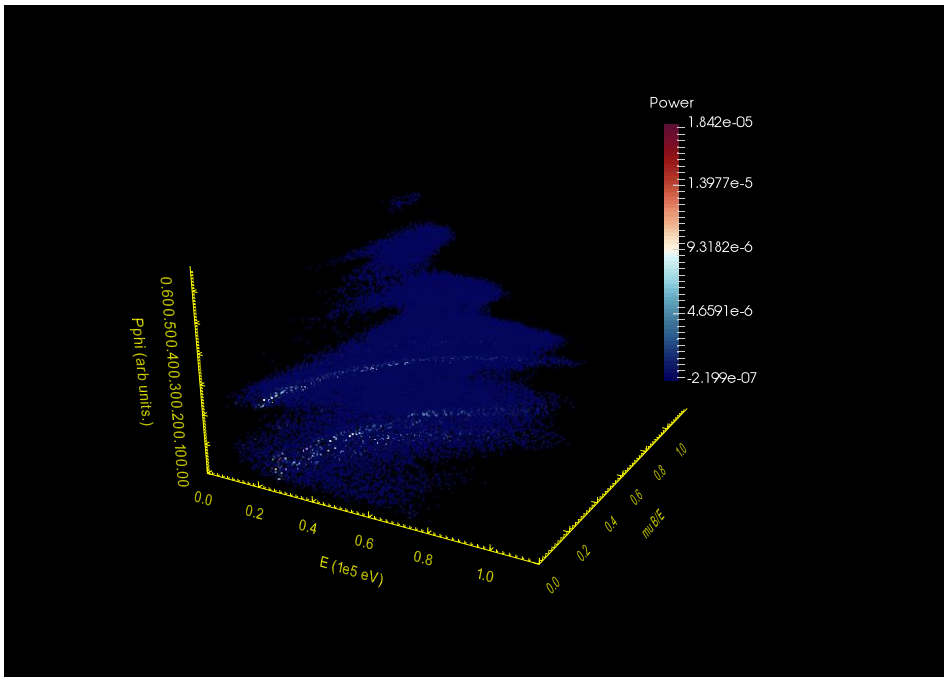

Figure 11: HALO computed wave-particle power transfer for particles in phase space. Bright lines correspond to the $\frac{V_A}{5}$ sideband TAE resonance condition

An important point to consider is: if core ion Landau damping is so high on JET, why were core localised Alfvenic modes driven by alphas observed on TFTR [4]? A quick analytical calculation is presented in Figure 12 showing a comparison between assuming a vacuum magnetic field of $B_0 = 3.4T$ as in the DD JET afterglow versus the same calculation with a TFTR vacuum magnetic field value of $B_0 = 5.1T$. The difference is a factor of ≈ 100 at the start of the afterglow. The interpretation is

clear; when raising the magnetic field, the Alfven eigenmodes propagate faster than the typical ion thermal speed, and so the resonant coupling between bulk thermal ions falls off rapidly.

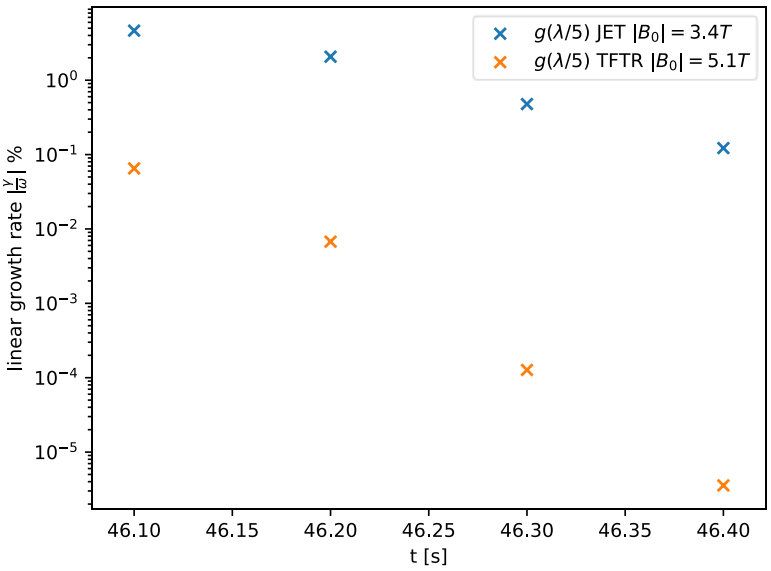

Figure 12: comparison of analytical approximation to ion Landau damping using different values of vacuum toroidal magnetic field.

Extrapolated kinetic alpha equilibrium from 96852 to DT

Having identified that the majority of the damping for the observed core TAEs occurs because of the thermal species, we extrapolate the conditions of our DD scenario to DT to predict whether these modes can be driven by alpha particles late in the afterglow when the core ion temperature has decreased. A standard extrapolation tool at JET is to perform interpretive modelling using the TRANSP code to obtain good agreement for predicted fusion rates and stored energy, then to re-run the interpretive case assuming a DT gas mixture. No thermal transport is modelled and only experimental profiles are used in the extrapolation. A number of similar afterglow experiments with small variations in fuelling and NBI timing were conducted in the absence of ICRH, the best performing in DD was shot 96852. This was chosen as the basis for extrapolation.

To obtain a smooth alpha distribution function, an isotropic slowing down distribution [39] was assumed of the form

$$F\left(E[eV],\mu[eV/T],P_\phi[Js]\right) = n\left(\psi\left(E,\mu,P_\phi\right)\right)\frac{N}{v^3+v_c^3}\,\mathrm{Erfc}\left[\frac{E-3.5\times10^6 eV}{106\times10^3\sqrt{T_{i0}[\mathrm{keV}]}}\right]$$

$$v_c \equiv \left(3\sqrt{\pi}\frac{m_e Z_1}{4}\right)^{\frac{1}{3}}\sqrt{\frac{2T_{e0}}{m_e}}$$

$$Z_1 = \frac{0.5}{2m_p}+\frac{0.5}{3m_p}$$

$$Ze\psi\left(E[eV],\mu[eV/T],P_\phi[Js]\right) \approx P_\phi - mR_0\sqrt{2(E-\mu B_0)/m} \qquad (14)$$

where the alpha density profile prediction $n(\psi)$ was taken from signal NFI from TRANSP using the lowest order approximation to the orbit-average poloidal flux, and only the on-axis temperature was used to avoid the complication of a spatial dependence in the normalization factor N.

Taking the integral of equation (14) produced a pressure which agrees with the TRANSP alpha stored energy signal UFASTPP and is shown in Figure 13.

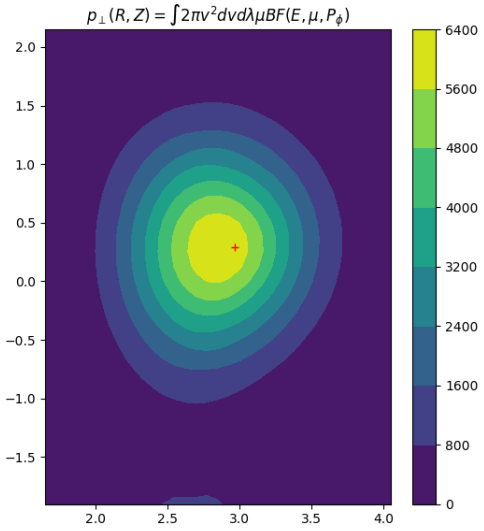

Figure 13: TRANSP derived alpha pressure during the high performance phase of 96852

DT predictions

Linear alpha drive calculations for the beginning of the afterglow were performed using the assumed slowing down form of the TRANSP alpha distribution function for the extrapolation of 96852. The result of the HALO calculation assuming the same eigenmodes as found for 92416 is presented in Figure 14. It is immediately obvious that no core modes, neither inboard nor outboard, are significantly driven by the alpha particles. It is likely that the broadness of the assumed alpha distribution is not supplying sufficient radial gradient to drive the core TAEs. Radial drive occurs when the fast ion diamagnetic frequency $n\omega_*$ at resonance exceeds the mode frequency ω where

$$\omega_* \equiv \left(\frac{\partial F}{\partial P_\phi}\right)_{E,\mu} \Big/ \left(\frac{\partial F}{\partial E}\right)_{\mu,P_\phi} \tag{15}$$

as expressed by equation (6). The larger orbit widths and Larmour radii of alpha particles would also favour broader modes found at lower toroidal mode number and radial position than those driven by ICRH. Even before considering damping mechanisms, we can predict that core localised TAEs will not be driven by alpha particles in the JET ITB afterglow. The strongest driven TAE, for the $n = 4{,}5{,}6$ modes considered, is located at $R = 3.55m$ just outside the usual location of the ITB (Figure 14). The maximum drive obtain was $\frac{\gamma_L}{\omega} = 0.7\%$ which is approximately an order of magnitude weaker than the drive predicted for ICRH. Although nonlinear results are not presented here, one can expect a factor of 100 lower saturation amplitude for a factor 10 lower linear drive.

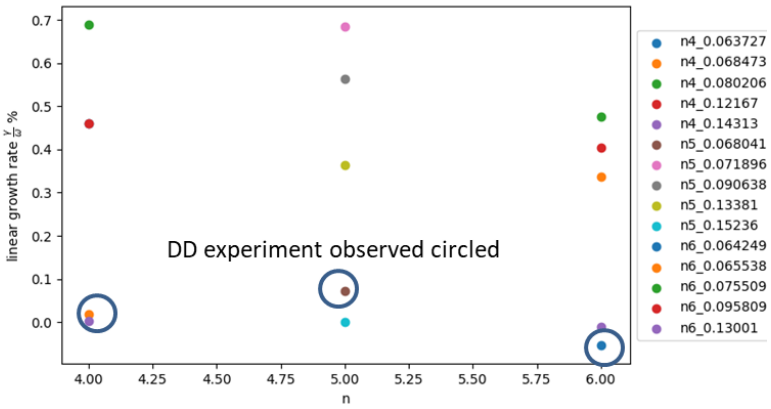

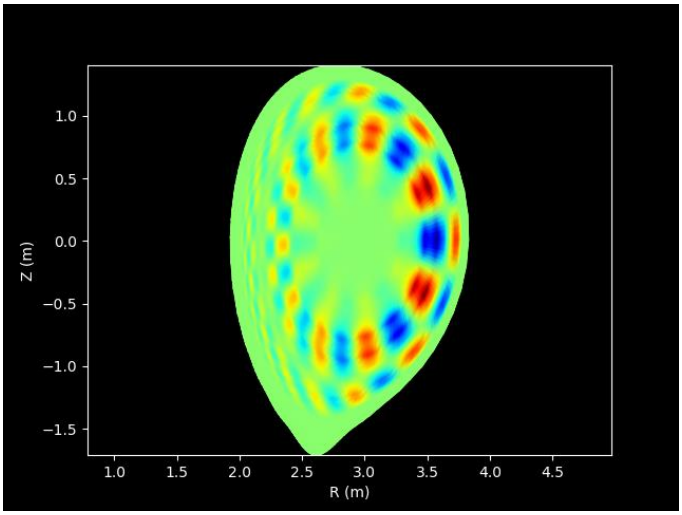

Figure 14:HALO alpha drive calculations for the eigenmodes from 92416 using the alpha pressure predicted for 96852 (above) and strongest alpha driven n=4 mode $\frac{\omega^2}{\omega_A^2} = 0.08$ *(below)*

These values of alpha drive can be compared with the ion Landau damping at the end of the afterglow. HALO was run using two thermal species D and T at 46.5s, again assuming the same eigenmodes and equilibrium. At this stage of the afterglow, the core ion temperature had dropped to a value of $T_i = 6\ keV$, compared with $T_i = 12keV$ at 46.1s. The results presented in Figure 15 show that modes found outside the core that experience stronger alpha drive also exhibit weaker Landau damping, as the local thermal ion density and temperature are also smaller closer to the edge. The strongest net linear growth rate, including only contributions from alpha drive and ion Landau damping, gives a mode even further out, peaking at R=3.7m. As expected, core localised modes observed in DD are those subject to the strongest ion Landau damping, owing to the peaked ion temperature and density in these ITB scenarios. The level of suppression of core localised modes means that the drive is an order-of-magnitude lower than the damping even at this later time during the afterglow.

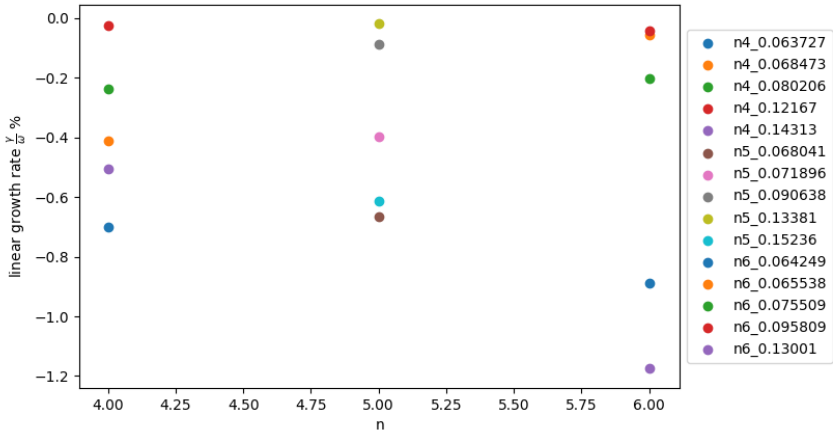

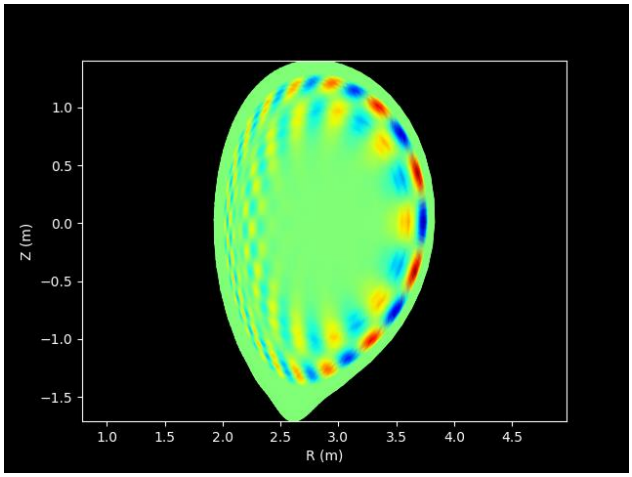

Figure 15: Ion Landau damping at 45.6s for shot 92416 assuming a bulk 50:50 DT plasma (above) and n=5 eigenmode $\frac{\omega^2}{\omega_A^2} = 0.09$ *with strongest net drive i.e.: alpha drive from 96852 minus ion Landau damping from 92416 (below)*

Conclusion

Detailed calculations of TAE stability during the JET ITB afterglow were performed using the best available data on the thermal and kinetic equilibrium. EFIT reconstructions using TRANSP fast pressure and measured thermal profiles together with low order representation for the flux functions gave good agreement with measured q-profiles in these scenarios. Subsequent incompressible MHD calculations on this equilibrium predicted both the frequency and position of modes observed. Perturbative calculations of ICRH drive and NBI damping were conducted using manual fits to Monte-Carlo data, leading to a likely overprediction of ICRH drive by a factor 1.2-1.3 given that mode destabilization occurred later than predicted. The modes predicted to experience the strongest drive are those observed in experiment, and modes predicted to be driven the least are not observed at all.

Calculations with HALO, CASTOR-K and GTC all confirm that the Maxwellian bulk plasma is responsible for strong damping of core modes and the main cause of the modes being suppressed during the high-performance phase of DD experiments, rather than the NBI ions. The damping was calculated to be of the order of $\frac{\gamma}{\omega} = 8\%$ at its peak. This strong damping in JET-like conditions is due to the $V_A/5$ sideband resonance often neglected in analytical results. Damping of this magnitude completely rules out alpha driven core localised TAEs during the entire afterglow (at least for n=4,5,6 considered in this work). However, given the broadness of the alpha distribution predicted by

TRANSP, TAEs which can be found closer to the edge experience significant alpha drive whilst being subject to lower ion Landau damping and may therefore be modestly unstable.

We anticipate that a likely follow-up study to this work will compute all known linear drive and damping contributions for every mode identified in linear and nonlinear regimes, as has been performed previously for ITER (e.g.: [31,32,40]). In this work, we have instead focused on the validity of reduced models to capture the essential measurable features in order to improve the credibility of such comprehensive predictions. Certainly, this work should be revisited when alpha particles are present and uncertainties in inputs to stability calculations are reduced. We should demand greater fidelity in our predictive capability in order to be of assistance to those making design decisions for future reactors. We should also explore large-scale uncertainty quantification techniques, propagating all the errors in the equilibrium distributions, leading to actionable predictions and more clarity on theory shortcomings.

The finding that ion Landau damping is a dominant factor in the stability of core TAEs echoes similar conclusions from the ITER work, and should be considered good news for fast ion confinement in burning plasma, even if it poses a significant challenge to overcome for driving TAEs with alphas in JET DT.

Acknowledgments

This work has been carried out within the framework of the EUROfusion Consortium and has received funding from the Euratom research and training programme 2014-2018 and 2019-2020 under grant agreement No 633053 and from the RCUK Energy Programme (grant number EP/P012450/1). The views and opinions expressed herein do not necessarily reflect those of the European Commission. To obtain further information on the data and models underlying this paper please contact PublicationsManager@ukaea.uk.

[1] Fasoli A, Gormenzano C, Berk H ., Breizman B, Briguglio S, Darrow D ., Gorelenkov N, Heidbrink W ., Jaun A, Konovalov S ., Nazikian R, Noterdaeme J-M, Sharapov S, Shinohara K, Testa D, Tobita K, Todo Y, Vlad G and Zonca F 2007 Chapter 5: Physics of energetic ions *Nucl. Fusion* **47** S264–84

[2] Dumont R J, Mailloux J, Aslanyan V, Baruzzo M, Challis C D, Coffey I, Czarnecka A, Delabie E, Eriksson J, Faustin J, Ferreira J, Fitzgerald M, Garcia J, Giacomelli L, Giroud C, Hawkes N, Jacquet P, Joffrin E, Johnson T, Keeling D, King D, Kiptily V, Lomanowski B, Lerche E, Mantsinen M, Meneses L, Menmuir S, McClements K, Moradi S, Nabais F, Nocente M, Patel A, Patten H, Puglia P, Scannell R, Sharapov S, Solano E R, Tsalas M, Vallejos P and Weisen H 2018 Scenario development for the observation of alpha-driven instabilities in JET DT plasmas *Nucl. Fusion* **58**

[3] Sharapov S E, Borba D, Fasoli A, Kerner W, Eriksson L G, Heeter R F, Huysmans G T A and Mantsinen M J 1999 Stability of alpha particle driven Alfvén eigenmodes in high performance JET DT plasmas *Nucl. Fusion* **39** 373–88

[4] Nazikian R, Fu G Y, Batha S H, Bell M G, Bell R E, Budny R V, Bush C E, Chang Z, Chen Y, Cheng C Z, Darrow D S, Efthimion P C, Fredrickson E D, Gorelenkov N N, Leblanc B, Levinton F M, Majeski R, Mazzucato E, Medley S S, Park H K, Petrov M P, Spong D A, Strachan J D, Synakowski E J, Taylor G, VonGoeler S, White R B, Wong K L and Zweben S J 1997 Alpha-particle-driven toroidal Alfven eigenmodes in the tokamak fusion test reactor *Phys. Rev. Lett.* **78** 2976–9

[5] Sauter O and Medvedev S Y 2013 Tokamak coordinate conventions: COCOS *Comput. Phys.*

Commun. **184** 293–302

[6] Cooper W and Wootton A 1982 βp analysis for Tokamak plasma with anisotropic pressure and mass flow *Plasma Phys.* **1183**

[7] Cheng C and Chance M 1986 Low-n Shear Alfvén Spectra in Axisymmetric Toroidal plasmas *Phys. Fluids* **29** 3695

[8] Candy J and Rosenbluth M N 1994 Nonideal theory of toroidal Alfvén eigenmodes *Phys. Plasmas* **1** 356–72

[9] Connor J W, Dendy R O, Hastie R J, Borba D, Huysmans G, Kerner W and Sharapov S 1994 Non-ideal effects on Toroidal Alfven Eigenmode stability *21st EPS Conference on Controlled Fusion and Plasma Physics* (Montpellier, France)

[10] Borba D and Kerner W 1999 CASTOR-K: Stability Analysis of Alfvén Eigenmodes in the Presence of Energetic Ions in Tokamaks *J. Comput. Phys.* **153** 101–38

[11] Gorelenkov N N, Cheng C Z and Fu G Y 1999 Fast particle finite orbit width and Larmor radius effects on low-n toroidicity induced Alfvén eigenmode excitation *Phys. Plasmas* **6** 2802–7

[12] Pinches S D, Appel L C, Candy J, Sharapov S E, Berk H L, Borba D, Breizman B N, Hender T C, Hopcraft K I, Huysmans G T A and Kerner W 1998 The HAGIS self-consistent nonlinear wave-particle interaction model *Comput. Phys. Commun.* **111** 133–49

[13] Fitzgerald M, Buchanan J, Akers R J, Breizman B N and Sharapov S E 2020 HALO: A full-orbit model of nonlinear interaction of fast particles with eigenmodes *Comput. Phys. Commun.* **252** 106773

[14] Mikhailovskii A B, Huysmans G T A, Kerner W O K and Sharapov S E 1997 Optimization of computational MHD normal-mode analysis for tokamaks *Plasma Phys. Reports* **23** 844–57

[15] Kerner W, Goedbloed J, Huysmans G, Poedts S and Schwarz E 1998 CASTOR: Normal-Mode Analysis of Resistive MHD Plasmas *J. Comput. Phys.* **142** 271–303

[16] Nyqvist R M and Sharapov S E 2012 Asymmetric radiative damping of low shear toroidal Alfvén eigenmodes *Phys. Plasmas* **19**

[17] Könies A, Briguglio S, Gorelenkov N, Fehér T, Isaev M, Lauber P, Mishchenko A, Spong D A, Todo Y, Cooper W A, Hatzky R, Kleiber R, Borchardt M, Vlad G, Biancalani A and Bottino A 2018 Benchmark of gyrokinetic, kinetic MHD and gyrofluid codes for the linear calculation of fast particle driven TAE dynamics *Nucl. Fusion* **58**

[18] Spong D a., Bass E M, Deng W, Heidbrink W W, Lin Z, Tobias B, Van Zeeland M a., Austin M E, Domier C W and Luhmann N C 2012 Verification and validation of linear gyrokinetic simulation of Alfvén eigenmodes in the DIII-D tokamak *Phys. Plasmas* **19** 082511

[19] Lauber P, Günter S, Könies a. and Pinches S D 2007 LIGKA: A linear gyrokinetic code for the description of background kinetic and fast particle effects on the MHD stability in tokamaks *J. Comput. Phys.* **226** 447–65

[20] Lin Z 1998 Turbulent Transport Reduction by Zonal Flows: Massively Parallel Simulations *Science (80-.).* **281** 1835–7

[21] Porcelli F, Stankiewicz R, Kerner W and Berk H L 1994 Solution of the drift-kinetic equation for global plasma modes and finite particle orbit widths *Phys. Plasmas* **1** 470–80

[22] Betti R and Freidberg J P 1992 Stability of Alfvén gap modes in burning plasmas *Phys. Fluids B*

Plasma Phys. **4** 1465–74

[23] Sharapov S E, Eriksson L G, Fasoli A, Gorini G, Källne J, Kiptily V G, Korotkov A A, Murari A, Pinches S D, Testa D S and Thomas P R 2008 Burning plasma studies at jet *Fusion Sci. Technol.* **53** 989–1022

[24] Nabais F, Aslanyan V, Borba D, Coelho R, Dumont R, Ferreira J, Figueiredo A, Fitzgerald M, Lerche E, Mailloux J, Mantsinen M, Rodrigues P, Porkolab M, Puglia P and Sharapov S E 2018 TAE stability calculations compared to TAE antenna results in JET *Nucl. Fusion* **58** 082007

[25] Brix M, Hawkes N C, Boboc A, Drozdov V and Sharapov S E 2008 Accuracy of EFIT equilibrium reconstruction with internal diagnostic information at JET *Rev. Sci. Instrum.* **79** 10F325

[26] Svensson J, Werner A and Contributors J-E 2008 Current tomography for axisymmetric plasmas *Plasma Phys. Control. Fusion* **50** 85002

[27] Hawryluk R J 1979 An empirical approach to tokamak transport *Physics of plasmas close to thermonuclear conditions* (Varenna, Italy: CEC, Brussels, 1980)

[28] Joffrin E, Challis C D, Conway G D, Garbet X, Gude A, Gunter S, Hawkes N C, Hender T C, Howell D F, Huysmans G T A, Lazzaro E, Maget P, Marachek M, Peeters A G, Pinches S D, Sharapov S E and Contributors J-E 2003 Internal transport barrier triggering by rational magnetic flux surfaces in tokamaks *Nucl. FUSION* **43** 1167–74

[29] Huysmans G T A, Goedbloed J P and Kerner W 1991 Isoparametric Bicubic Hermite Elements for Solution of the Grad-Shafranov Equation *Int. J. Mod. Phys. C* **02** 371–6

[30] Berk H L, Van Dam J W, Borba D, Candy J, Huysmans G T A and Sharapov S 1995 More on core-localized toroidal Alfvén eigenmodes *Phys. Plasmas* **2** 3401–6

[31] Fitzgerald M, Sharapov S E, Rodrigues P and Borba D 2016 Predictive nonlinear studies of TAE-induced alpha-particle transport in the Q = 10 ITER baseline scenario *Nucl. Fusion* **56** 112010

[32] Rodrigues P, Figueiredo A, Ferreira J, Coelho R, Nabais F, Borba D, Loureiro N F, Oliver H J C and Sharapov S E 2015 Systematic linear-stability assessment of Alfvén eigenmodes in the presence of fusion α-particles for ITER-like equilibria *Nucl. Fusion* **55** 083003

[33] Hedin J, Hellsten T, Eriksson L G and Johnson T 2002 The influence of finite drift orbit width on ICRF heating in toroidal plasmas *Nucl. Fusion* **42** 527–40

[34] Hirvijoki E, Asunta O, Koskela T, Kurki-Suonio T, Miettunen J, Sipilä S, Snicker a. and Äkäslompolo S 2014 ASCOT: Solving the kinetic equation of minority particle species in tokamak plasmas *Comput. Phys. Commun.* **185** 1310–21

[35] Di Troia C 2012 From the orbit theory to a guiding center parametric equilibrium distribution function *Plasma Phys. Control. Fusion* **54**

[36] Di Troia C 2015 Bayesian derivation of plasma equilibrium distribution function for tokamak scenarios and the associated Landau collision operator *Nucl. Fusion* **55**

[37] Seo J, Kim J, Mailloux J, Dumont R J, Fitzgerald M, Sharapov S E, Keeling D L, Koechl F, Casson F J, Lee C Y, Hahm T S and Na Y-S 2020 Parametric study of linear stability of toroidal Alfvén eigenmode in JET and KSTAR *Nucl. Fusion* **60** 066008

[38] Todo Y and Sato T 1998 Linear and nonlinear particle-magnetohydrodynamic simulations of the toroidal Alfvén eigenmode *Phys. Plasmas* **5** 1321

[39] Gaffey J D 1976 Energetic ion distribution resulting from neutral beam injection in tokamaks *J. Plasma Phys.* **16** 149

[40] Figueiredo A C A, Rodrigues P, Borba D, Coelho R, Fazendeiro L, Ferreira J, Loureiro N F, Nabais F, Pinches S D, Polevoi A R and Sharapov S E 2016 Comprehensive evaluation of the linear stability of Alfvén eigenmodes driven by alpha particles in an ITER baseline scenario *Nucl. Fusion* **56**